RSC Advances

PAPER

View Article Online
View Journal | View Issue

Cite this: *RSC Adv.*, 2026, **16**, 29807

Electrospun collagen/hyaluronic acid dressing co-loaded with EGF and bFGF for enhanced diabetic wound healing

Liang Wu,†[a] Wei Wang,†[a] Linxinyi Chen,†[b] Duohui Li,[a] Yijun Ke,[a] Yanghui Xu,[a] Bo Zhu,[a] Fangqi Hu,*[a] Lishang Dai *[b] and Xiwu Shi*[a]

Chronic non-healing wounds are a major complication of diabetes and require advanced therapeutic strategies. Although epidermal growth factor (EGF) and basic fibroblast growth factor (bFGF) are known to promote tissue regeneration, their poor stability and short half-life have severely restricted clinical translation. To overcome these challenges, a collagen/hyaluronic acid dressing loaded with EGF and bFGF (CH-EGF/bFGF) was prepared *via* electrospinning. CH-EGF/bFGF exhibited a fibrous network-like entanglement and possessed good water retention and mechanical properties. *In vitro* experiments, it was observed that CH-EGF/bFGF not only had good biosafety but also promoted the adhesion, proliferation, and migration of HaCaT cells through activation of the ERK1/2 and p38 MAPK signaling pathways. Furthermore, CH-EGF/bFGF effectively accelerated the wound-healing process in db/db diabetic mice, and markedly enhanced the expression of vascular endothelial growth factor, Ki67, CD31, alpha-smooth muscle actin, collagen I, and collagen III at the wound site. This study achieves dual growth factor stabilization and controlled release through an electrospun biomimetic matrix that simultaneously mimics the extracellular matrix and maintains a moist wound-healing milieu. In conclusion, CH-EGF/bFGF demonstrated promising potential for promoting diabetic wound healing, offering a novel and viable therapeutic approach for the clinical management of diabetic wounds.

Received 4th December 2025
Accepted 7th March 2026

DOI: 10.1039/d5ra09378c

rsc.li/rsc-advances

1. Introduction

Diabetes mellitus is recognized as a severe chronic metabolic disorder,[1] affecting approximately 463 million people worldwide.[2] One of its major complications is the development of chronic, non-healing wounds, which are primarily characterized by fibroblast dysfunction, persistent inflammation, impaired epithelialization, insufficient chemokine production, and inadequate angiogenesis.[3] These characteristics collectively result in difficulties in wound healing, significantly compromising the physical and mental health of patients. Although various treatment strategies for chronic non-healing wounds have been proposed, including debridement, decompression, endovascular therapy, surgical interventions to promote vascular regeneration, and the use of growth factors to facilitate wound healing, the healing of patients' wounds often remains slow and may rapidly deteriorate. Consequently, there is an urgent need to explore more rational treatment options.

Pro-inflammatory cytokines and matrix metalloproteinases are highly expressed at diabetic wound sites, which inhibit both the expression and activity of endogenous growth factors.[4] As a result, angiogenesis and wound repair are significantly impaired and proceed at a markedly slow pace. Among the affected growth factors, the regulation of epidermal growth factor (EGF)[5] and basic fibroblast growth factor (bFGF)[6] is dysregulated during the diabetic wound healing process. EGF can stimulate the proliferation and migration of keratinocytes in diabetic wounds, promoting dermal regeneration.[7] Meanwhile, bFGF has the ability to induce angiogenesis and facilitate wound repair.[8] However, despite the promising therapeutic potential of EGF and bFGF, their clinical translation still faces several intrinsic limitations. Both growth factors are susceptible to rapid proteolytic degradation and exhibit short *in vivo* half-lives in the protease-rich microenvironment of diabetic wounds, resulting in insufficient local bioavailability.[9] In addition, their therapeutic efficacy is highly dependent on dosage and timing, and uncontrolled administration may lead to abnormal tissue proliferation or ineffective angiogenic responses. Although various delivery systems have been developed to improve their stability and retention, achieving the synchronized regulation of epithelial regeneration and angiogenesis remains challenging.[10,11] Notably, single-factor delivery strategies are often insufficient to simultaneously regulate epithelial regeneration and angiogenesis during wound healing. Therefore, the combined

[a]*Anqing Municipal Hospital, Anqing 246000, PR China. E-mail: shixiwu0905@163.com; lishang2016@wmu.edu.cn; hfxgyh@163.com*

[b]*School of Pharmaceutical Sciences, Wenzhou Medical University, Wenzhou 325035, PR China*

† These authors contributed equally to this work.

delivery of EGF and bFGF may provide complementary biological functions and enable spatiotemporal regulation of tissue regeneration.

In this context, natural biomaterials such as hyaluronic acid (HA) and collagen I have garnered significant attention due to their excellent biocompatibility, biodegradability, and structural similarity to the native extracellular matrix (ECM).[12] HA, a glycosaminoglycan found in the ECM, has been demonstrated to regulate the recruitment of immune cells on the vascular wall and endothelial cell layer,[13] thereby playing a crucial role in angiogenesis and promoting wound healing. It has been approved by the FDA for widespread use in wound dressings, including sponges, films, hydrogels, and electrospun membranes.[14] In addition, effective wound healing requires the involvement of collagen. Collagen I has been reported to effectively enhance the proliferation and migration of endothelial cells, contributing positively to the vascularization process during wound repair.[15] It is also regarded as an ideal material for constructing angiogenesis scaffolds.[16] Among the available fabrication techniques, electrospinning stands out as a reliable approach for producing nanofibrous scaffolds that closely mimic the native ECM. Electrospun membranes offer high porosity, large surface area, and tunable fiber morphology, which collectively provide a conductive microenvironment for sustained release of bioactive factors.[17] Based on these considerations, it is hypothesized that a wound dressing cross-linked with collagen I and HA (CH), prepared using electrospinning technology and loaded with EGF and bFGF, may be beneficial for accelerating the healing of diabetic wounds.

To verify this hypothesis, in the present study, the ratio of collagen I to HA was optimized, and electrospinning technology was employed to prepare CH dressing loaded with EGF and bFGF (CH-EGF/bFGF). Subsequently, the microstructure, biosafety, degradability, absorbency, and drug release properties were characterized, and the repair effects on db/db diabetes mouse wounds were evaluated. This study aimed to offer a potential therapeutic strategy for the clinical management of diabetic wounds.

2. Materials and methods

2.1. Cell culture

Human immortalized epidermal cells (HaCaT, YB-ATCC-2249, ATCC) were purchased from the American Type Culture Collection (ATCC). They were cultured in DMEM medium (D0822, Sigma-Aldrich) supplemented with 10% fetal bovine serum and 1% penicillin–streptomycin solution, and incubated in a 37 °C, 5% CO_2 incubator.

2.2. Animals

db/db mice (male, 12 weeks old) were purchased from Sipeifu (Beijing) Biotechnology Co., Ltd. and housed in a sterile environment with a 12 h light/12 h dark cycle. db/db mice were used as a model of type II diabetes. They were allowed ad libitum access to food and water. All experimental procedures were conducted in accordance with the ARRIVE 2.0 guidelines and approved by the Experimental Animal Ethics Committee of Wenzhou Medical University (wydw2024-0588).

2.3. Preparation of CH dressing

Collagen I (CC050, Sigma-Aldrich) and HA (924474, Sigma-Aldrich) were dissolved in 5 mL of hexafluoroisopropanol solution (H107501, Aladdin) at three different ratios: CH1 (collagen I : HA = 2 : 1), CH2 (collagen I : HA = 4 : 1), and CH3 (collagen I : HA = 8 : 1). Among them, the CH2 formulation showed the optimal physicochemical properties in preliminary screening. Therefore, it was selected for subsequent experiments. For the CH2 formulation, the final concentrations of collagen I and HA in the spinning solution were 8% (w/v) and 2% (w/v), respectively, resulting in a total polymer concentration of 10% (w/v). The solutions were stirred at 4 °C for 1 hour until the collagen I and HA were completely dissolved, forming spinning solutions. The spinning solutions were then aspirated into a 10 mL syringe equipped with a 21 G needle. The syringe, along with an insulated wire and an iron clip, was used to connect the electrostatic high-voltage generator to the needle. A piece of aluminum foil was attached to the collector using double-sided tape for electrospinning the fibers. The spinning parameters were adjusted as follows: the voltage was set to 10–11 kV, the needle flow rate was controlled at 0.36 mL h^{-1}, and the distance between the needle tip and the collector plate was set to 10 cm. The spinning temperature was maintained at 25 °C. Under the influence of high voltage, the spinning solution was ejected in an electric field to form fibers that were deposited on the collector, resulting in the formation of collagen/hyaluronic acid dressings.

For growth factor loading, concentrated solutions of bFGF (HY-P5321, MCE) and EGF (HY-P7067, MCE) (50 μg mL^{-1}) were added dropwise into the spinning solutions. Specifically, 40 μL of each solution was added, corresponding to 2 μg of bFGF and 2 μg of EGF in the spinning solution. Subsequently, bFGF and EGF were loaded onto the CH membranes through electrospinning to obtain CH-EGF/bFGF.

2.4. Microscopic morphology characterization of CH fibrous membranes

The prepared CH, CH-EGF, CH-bFGF, and CH-EGF/bFGF fibrous membranes were adhered to a copper plate using conductive adhesive, followed by gold sputtering treatment. Their microscopic structures were then observed under a scanning electron microscope (SEM, SU8600, Hitachi).

2.5. Determination of water absorbency and water retention

CH1, CH2, and CH3 dressings (1 × 1 cm) were taken, and their initial masses were recorded as m_0. The dressings were immersed in water (5 mL, 25 °C), and the mass of each sample was measured at 1 h, 2 h, 4 h, 6 h, 8 h, 10 h, 12 h, 16 h, 24 h, 36 h, and 48 h, respectively, denoted as m_i. The water absorbency ratio at different time points was calculated using the formula: $I = (m_i - m_0)/m_0$ to evaluate the water absorbency performance of the dressings.

Similarly, CH1, CH2, and CH3 dressings (1 × 1 cm) were taken and immersed in water (5 mL, 25 °C) for 24 hours. The

mass of the dressings at this point was recorded as m_e. The samples were then placed in a ventilated environment at 25 °C, and the mass of each dressing was measured at 3 h, 6 h, 12 h, 18 h, 24 h, 36 h, and 48 h, respectively, denoted as m_t. The water retention performance of the dressing was evaluated using the formula: $G = (m_t - m_0)/(m_e - m_0) \times 100\%$.

2.6. Mechanical property testing

The CH1, CH2, and CH3 nanofiber membranes were each cut into strips measuring 20 mm × 8 mm. A universal testing machine (AGX-V2, Shimadzu) was used to test their mechanical properties, with an experimental loading speed of 2.5 mm min^{-1}.

2.7. Infrared spectroscopy measurement

A small amount of HA, Collagen I, CH2, CH-EGF, CH-bFGF, and CH-EGF/bFGF was taken for tablet compression. Subsequently, Fourier transform infrared spectroscopy (FTIR) analysis was performed using a Fourier Transform Infrared Spectrometer (NICOLET is20, Thermo Scientific). The wavenumber range for the test was set between 4000–400 cm^{-1} to verify whether HA and collagen I were successfully cross-linked.

2.8. Measurement of degradation rate

A small amount of CH-EGF/bFGF was taken and weighed (G_0). It was then immersed in PBS buffer (P7059, Sigma-Aldrich) and placed in an incubator maintained at 37 °C. The samples were taken out on the 1st, 4th, 7th, 10th, 13th, 16th, 19th, and 21st days, respectively, transferred to an oven, and dried for 24 hours before being weighed again (G_d). The degradation rate of the nanofiber membrane was calculated using the following formula:

$$\text{Degradation rate (\%)} = (G_0 - G_d) / G_0 \times 100\%$$

2.9. Cell cytotoxicity and proliferation assay

For cell cytotoxicity assay, HaCaT cells (1×10^4) were seeded into a 96-well plate and pre-incubated in an incubator (37 °C, 5% CO_2) for 48 hours. Subsequently, different sizes of CH-EGF/bFGF (0, 1 × 1, 3 × 3, 5 × 5, and 8 × 8 mm) were added to the 96-well plate, and the plate was incubated in the incubator for either 24 hours or 48 hours. Next, 10 μL of CCK-8 solution (C0038, Beyotime) was added to each well, and the incubation was continued for an additional 1 hour. Finally, the absorbance at 450 nm was measured using a microplate reader (INFINITE M 200 PRO, TECAN).

For proliferation assessment, HaCaT cells were seeded at 2×10^3 cells per well and incubated overnight. Membranes (5 × 5 mm) were added, and CCK-8 reagent was applied after 24 and 48 h as described above to quantify cell proliferation rates.

2.10. Cell adhesion experiment

CH2 (5 × 5 mm) and CH-EGF/bFGF (5 × 5 mm) were separately adhered to the bottom of a 24-well culture plate and sterilized under a UV lamp for 1 hour. Each well was then supplemented with 1 mL of high-glucose DMEM containing 10% FBS and 1% penicillin/streptomycin. Subsequently, HaCaT cells (2×10^4) were seeded into the 24-well plate and cultured for 24 and 48 hours, after which the culture medium was discarded. Each well was then supplemented with 0.6 mL of fluorescein diacetate solution (5 μg mL^{-1}, F7378, Sigma-Aldrich) for staining, and the staining process lasted for 5 minutes. Upon completion of staining, the dye was removed, and 1 mL of PBS solution was added to each well. Finally, an inverted fluorescence microscope (Axio Observer 5, Zeiss) was used to examine the adhesion and growth of HaCaT cells on CH2 and CH-EGF/bFGF.

2.11. Wound healing assay

HaCaT cells were seeded into 6-well plates at a density of 2×10^5 cells per well and cultured to 90% confluence. A linear scratch was created using a pipette tip across the cell monolayer. Cells were washed with PBS to remove debris and then incubated with fresh medium containing CH2, CH-EGF, CH-bFGF, or CH-EGF/bFGF membranes (5 × 5 mm). Images of the wound area were captured at 48 h using an inverted microscope (Axio Observer 5, Zeiss). The migration rate was quantified using ImageJ software.

2.12. Western blot analysis

HaCaT cells were seeded in 6-well plates at a density of 2×10^5 cells per well and allowed to attach overnight. The cells were then treated with CH2, CH-EGF, CH-bFGF, or CH-EGF/bFGF (5 × 5 mm) for 24 hours. After treatment, the cells were washed twice with cold PBS and lysed with RIPA buffer (P0013B, Beyotime). The lysates were incubated on ice for 30 min and centrifuged at 12 000 rpm for 15 min at 4 °C. The supernatants were collected, and protein concentrations were determined using a BCA assay kit (P0012, Beyotime). Equal amounts of protein were separated by 10% SDS-PAGE. Proteins were then transferred onto PVDF membranes (IPVH00010, Millipore). Membranes were blocked with 5% non-fat milk for 1 h at room temperature and incubated overnight at 4 °C with primary antibodies: p-ERK1/2 (1 : 1000, #4370, Cell Signaling Technology), ERK1/2 (1 : 1000, #4695, CST), p-p38 MAPK (1 : 1000, #4511, CST), and p38 MAPK (1 : 1000, #8690, CST). GAPDH (1 : 5000, ab8245, Abcam) was used as a loading control. Then, membranes were incubated with HRP-conjugated secondary antibody (1 : 5000, A0208, Beyotime) for 1 h at room temperature. Protein bands were visualized using an enhanced chemiluminescence kit (P0018FS, Beyotime). Band intensities were quantified with ImageJ.

2.13. Hemolysis assay

Blood (100 μL) was collected from the heart of db/db mice using cardiac puncture and mixed with an appropriate amount of 3.8% sodium citrate solution (1613859, Sigma-Aldrich) to obtain fresh anticoagulated murine blood. The blood was then centrifuged at 3000 rpm for 10 minutes, and the supernatant was discarded. The erythrocytes at the bottom were washed with normal saline (52455, Sigma-Aldrich). Subsequently, the

erythrocytes were resuspended in normal saline to obtain a 2% erythrocyte suspension.

The following solutions and samples were added to six empty centrifuge tubes, respectively: 500 μL of distilled water (H_2O group), 500 μL of normal saline (NS group), CH2 (5 × 5 mm) + 500 μL of normal saline (CH2 group), CH-EGF (5 × 5 mm) + 500 μL of normal saline (CH-EGF group), CH-bFGF (5 × 5 mm) + 500 μL of normal saline (CH-bFGF group), and CH-EGF/bFGF (5 × 5 mm) + 500 μL of normal saline (CH-EGF/bFGF group). The centrifuge tubes were then incubated in a 37 °C thermostatic shaker for 30 minutes. Afterward, erythrocyte suspension was added to each centrifuge tube, mixed well, and incubated in the 37 °C thermostatic shaker for an additional 60 minutes. Upon completion of incubation, the fibers in the centrifuge tubes were removed, and the samples were centrifuged (3000 rpm, 5 minutes). The supernatant was aspirated, and the absorbance was measured at 545 nm, with the results recorded.

2.14. Delivery rate of bFGF and EGF

The release rates of bFGF and EGF from CH2 were detected using ELISA kits. In brief, a certain amount of CH-EGF, CH-bFGF, and CH-EGF/bFGF was taken and added to 1.5 mL EP tubes. 1 mL of PBS solution was then added to each EP tube, and the tubes were placed in a 4 °C refrigerator. Subsequently, the supernatant was collected at 0 d, 0.02 d, 0.04 d, 0.08 d, 0.25 d, 0.5 d, 1 d, 3 d, 5 d, and 7 d, respectively, and an equal volume of PBS was added to each collected sample. The collected samples were stored in a −80 °C refrigerator. The amounts of bFGF and EGF released from CH2 in the collected solutions were determined using an ELISA kit (J&L Biological, China).

2.15. Preparation of the mouse wound model

After a one-week acclimation period, db/db mice were subjected to tail vein puncture for blood collection to measure their blood glucose levels three times (following a 4 hours fast, with one-day intervals between measurements). db/db mice with an average blood glucose level greater than 13.0 mmol L^{-1} were selected as the model group for subsequent experiments.

The selected db/db mice were anesthetized with isoflurane and then secured onto the operating table. The hair on their backs was removed using a hair clipper and hair removal cream, and the skin on their backs was disinfected with alcohol. Subsequently, a full-thickness skin wound with a diameter of 10 mm was created on the back of each mouse using a circular skin punch.

2.16. Grouping and treatment of mice

All db/db mice subjected to wound modeling were randomly divided into five groups ($n = 8$), namely: the Blank group (treated with normal saline), the CH2 group (loaded with 10 × 10 mm CH2), the CH-EGF group (loaded with 10 × 10 mm CH-EGF), the CH-bFGF group (loaded with 10 × 10 mm CH-bFGF), and the CH-EGF/bFGF group (loaded with 10 × 10 mm CH-EGF/bFGF). Each group received treatment once every three days. The 10 mm diameter CH2, CH-EGF, CH-bFGF, and CH-EGF/bFGF dressings were closely applied to the wounds, and then covered with a waterproof transparent polyurethane film dressing. Elizabethan collars were put on each mouse to prevent interference with the wound while allowing free movement.

On the 0th, 3rd, 7th, 10th, 14th, and 21st days post-surgery, photographs of the skin wounds of mice in each group were taken. The wound sizes were calculated using Image-Pro software, and the healing rates were subsequently determined.

2.17. H&E staining

On the 7th and 21st days post-surgery, four mice from each group were euthanized, and the wound tissues were harvested. The tissues were fixed with 4% paraformaldehyde, dehydrated using a gradient of ethanol, and then embedded in paraffin and sectioned. The tissue sections were stained according to the H&E staining kit (C0105S, Beyotime). Specifically, the sections were immersed in hematoxylin staining solution for 10 minutes, after which they were removed and rinsed with running water. Subsequently, the sections were immersed in hydrochloric acid-ethanol (C0163S, Beyotime) for 3 seconds and then rinsed again with running water. Next, the sections were stained in eosin solution for 2 minutes. Finally, after undergoing dehydration, clarification, and mounting processes, the sections were observed under a microscope (Ni-U, Nikon).

2.18. Masson staining

To detect deposited collagen and keratin, tissue sections were stained using a Masson staining kit (C0189S, Beyotime). Specifically, the sections were immersed in hematoxylin staining solution for 5 minutes and then differentiated with hydrochloric acid-ethanol for 3 seconds. Subsequently, the sections were stained in a ponceau-acid fuchsin solution for 5 minutes. After rinsing with running water, the sections were treated with an aqueous solution of phosphomolybdic acid for 5 minutes. Next, the sections were counterstained with aniline blue solution for 5 minutes. Finally, after undergoing dehydration, clarification, and mounting processes, the sections were observed under a microscope.

2.19. Immunohistochemistry (IHC)

Tissue sections were washed with PBS and then immersed in 3% H_2O_2 for 15 minutes. After blocking with blocking solution for 1 hour, the sections were incubated with primary antibodies overnight at 4 °C. The sections were then rinsed with PBS and co-incubated with a horseradish peroxidase (HRP)-conjugated goat anti-rabbit secondary antibody (A0208, Beyotime) at 37 °C for 30 minutes. Subsequently, the sections were developed with 3,3′-diaminobenzidine (DAB, ST3205, Beyotime) for 15 minutes, followed by dehydration, clarification, and mounting. The differences among the sections from each group were compared under a microscope, and the positive areas were quantitatively analyzed using ImageJ. The primary antibodies used included an anti-Ki67 antibody (1 : 200, SAB5600249, Sigma-Aldrich), an anti-collagen I antibody (1 : 200, HPA011795, Sigma-Aldrich), an anti-VEGF antibody (1 : 200, ABS82, Sigma-Aldrich), and an anti-collagen III antibody (1 : 200, HPA007583, Sigma-Aldrich).

2.20. Immunofluorescence

Tissue sections were placed in citrate antigen retrieval solution and maintained at a sub-boiling temperature for 10 minutes. Subsequently, the sections were incubated in blocking solution for 1 hour and then with primary antibodies overnight at 4 °C. On the following day, an AF647-labeled secondary antibody (A0468, Beyotime) was added, and the sections were further incubated at room temperature for 1 hour. Finally, after dehydration and clarification, the sections were mounted, and fluorescence images were captured using a fluorescence microscope, and the positive areas were quantitatively analyzed using ImageJ. The primary antibodies used included an anti-CD31 antibody (1 : 200, SAB5700639, Sigma-Aldrich) and an anti-α-SMA antibody (1 : 200, A5228, Sigma-Aldrich).

2.21. Statistical analysis

All experiments were repeated at least three times. Statistical analysis and graph plotting of the data were performed using GraphPad Prism software. All data were presented as the mean ± standard deviation (SD). Inter-group differences were analyzed using one-way analysis of variance (ANOVA), followed by *post hoc t*-tests. A *P*-value of less than 0.05 was considered statistically significant.

3. Results

3.1. Preparation and characterization of CH-EGF/bFGF

To screen the optimal ratio of collagen to HA, mixtures of collagen I/HA at different ratios, namely CH1, CH2, and CH3, were initially prepared. The microstructures of the electrospun membranes were observed using SEM. The results indicated that the electrospun membrane formed by CH2 exhibited a uniform fibrous network entanglement (Fig. 1A). To further verify the rationality of the selected electrospinning parameters, the effect of spinning voltage on fiber morphology was evaluated. SEM observations revealed that at 6 or 8 kV, insufficient electrostatic force resulted in sparse fiber formation (Fig. S1A and B). At 12 or 14 kV, excessive electric field strength caused partial fiber fusion and irregular network structures (Fig. S1C and D). In contrast, electrospinning at 10–11 kV produced uniform, smooth, and bead-free nanofibers with a continuous fibrous network (Fig. 1A). Subsequently, the water absorption and water retention capacities of CH1, CH2, and CH3 were determined. The results demonstrated that CH2 outperformed CH1 and CH3 in both water absorption and water retention capacities (Fig. 1B and C). In subsequent tensile strength experiments, it was also found that CH2 possessed the optimal elongation properties (Fig. 1D), making it more suitable for wound dressings. The elastic modulus of CH1, CH2, and CH3 was calculated as 5.27 MPa, 4.76 MPa, and 4.26 MPa, respectively. SEM images were further analyzed to measure nanofiber diameters, revealing mean diameters of 0.212 ± 0.037 μm for CH1, 0.222 ± 0.015 μm for CH2, and 0.254 ± 0.081 μm for CH3. Therefore, CH2 was selected as the carrier material for EGF and bFGF in subsequent experiments. A schematic illustration of the preparation process of CH-EGF/bFGF is shown in Fig. 1E.

Subsequently, SEM was used to observe the microstructure of CH-EGF/bFGF. The results revealed that the fibers had a smooth surface and formed numerous physical entanglements among themselves (Fig. 1F). To further verify the successful cross-linking of HA and collagen I in CH2, FTIR was employed. The results revealed that the FTIR spectrum of CH2 displayed characteristic absorption peaks of both HA and collagen I (Fig. 1G), strongly confirming the successful cross-linking of HA and collagen I. Specifically, the broad absorption band at approximately 3200–3500 cm^{-1} was attributed to O–H and N–H stretching vibrations. The peaks near 1650 cm^{-1} (amide I band) and 1540 cm^{-1} (amide II band) corresponded to the characteristic protein backbone vibrations of collagen I. In addition, the absorption peak at approximately 1040–1080 cm^{-1} was assigned to the C–O–C and C–O stretching vibrations of the polysaccharide structure of HA. Additionally, in the CH-EGF group, a shift of the amide I/II bands towards lower wavenumbers was observed, along with the emergence of a weak peak near 1510 cm^{-1}, indicating the incorporation of EGF. In the CH-bFGF group, a slight enhancement of the peak near 1040 cm^{-1} (due to the overlap of the sulfation site and the amide III band) was noted, indicating the successful loading of bFGF. In the CH-EGF/bFGF group, a composite effect was observed, characterized by a shift of the amide I/II bands towards lower wavenumbers, the appearance of a weak peak near 1510 cm^{-1}, and a slight enhancement of the amide III band peak, revealing the co-loading of EGF and bFGF.

3.2. Evaluation of the degradation, biocompatibility, sustained release, and cell adhesion-promoting effects of CH-EGF/bFGF

To characterize the *in vitro* degradation of CH-EGF/bFGF, its degradation rate over a 21 days period was measured. The results indicated that the degradation rate of CH-EGF/bFGF was relatively fast within the first 0–7 days. From the 8th to the 17th day, the degradation rate tended to level off, reaching nearly 50% by day 21 (Fig. 2A). Subsequently, the biological safety of CH-EGF/bFGF was evaluated through cytotoxicity and hemolysis assays. The results demonstrated that CH-EGF/bFGF did not significantly affect the viability of HaCaT cells within 24 hours and 48 hours (Fig. 2B). The hemolysis assay further confirmed that CH-EGF/bFGF possessed good biological safety (Fig. 2C).

In addition, the drug release performance of CH-EGF/bFGF was measured. The results showed that the drugs loaded in CH2 could achieve a slow release within the first 1–7 days (Fig. 2D). After 7 days, the release curve had already reached a stable state, and the cumulative release rate had entered a plateau phase (Fig. S2). Then, the effect of CH-EGF/bFGF on the adhesion and growth of HaCaT cells was measured by FDA staining. The results demonstrated that after 48 hours, the fluorescence intensity in the CH-EGF/bFGF group was significantly higher than that in the CH2 group. This indicated that HaCaT cells could adhere and grow on the dressings (Fig. 2E), and CH-EGF/bFGF could effectively promote the growth of HaCaT cells.

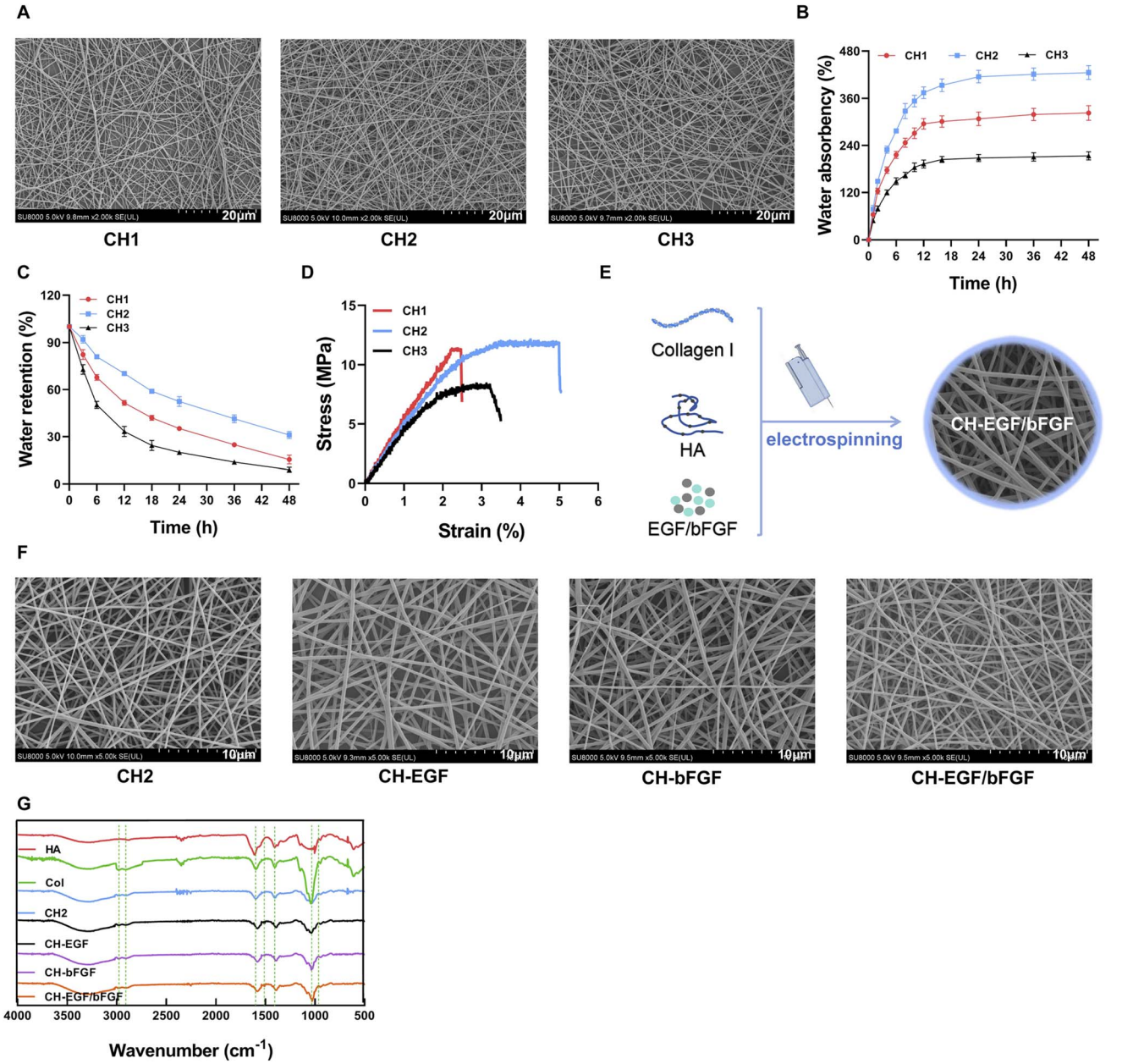

Fig. 1 Preparation and characterization of CH-EGF/bFGF dressings. (A) SEM images of the electrospun membrane structures of CH1, CH2, and CH3 (scale bar, 20 μm). (B) Water absorption tests of CH1, CH2, and CH3, $n = 3$. (C) Water retention tests of CH1, CH2, and CH3, $n = 3$. (D) Biomechanical properties of CH1, CH2, and CH3, $n = 3$. (E) The preparation process of CH-EGF/bFGF. (F) SEM image of the CH-EGF/bFGF structure (scale bar, 5 μm). (G)The successful cross-linking of HA, Col, CH2, CH-EGF, CH-bFGF, and CH-EGF/bFGF was confirmed by FTIR.

3.3. CH-EGF/bFGF promoted the healing of chronic skin wounds in diabetic mice

Through the evaluation of wound healing (Fig. 3), it was observed that wounds treated with CH-EGF/bFGF nanofiber membranes exhibited a significant reduction in area, with a healing rate of 79.7% by the seventh day. By the 14th day, the healing rates of the Blank, CH2, CH-EGF, and CH-bFGF groups were 79.04 ± 6.05%, 84.66 ± 0.90%, 85.51 ± 1.30%, and 88.89 ± 1.07%, respectively. In contrast, the CH-EGF/bFGF group achieved a healing rate of 92.81 ± 2.31%, demonstrating its remarkable therapeutic efficacy.

These findings suggested that CH-EGF/bFGF was effective in promoting wound healing in type 2 diabetic mice. In addition, dressings loaded with EGF or bFGF alone also exhibited certain therapeutic effects on the wounds. However, their therapeutic outcomes were less pronounced when compared to those observed in the CH-EGF/bFGF group.

In addition, H&E staining results revealed that on the 7th day of treatment, severe inflammatory responses were observed in the wound sites of mice from the Blank group. In some wound

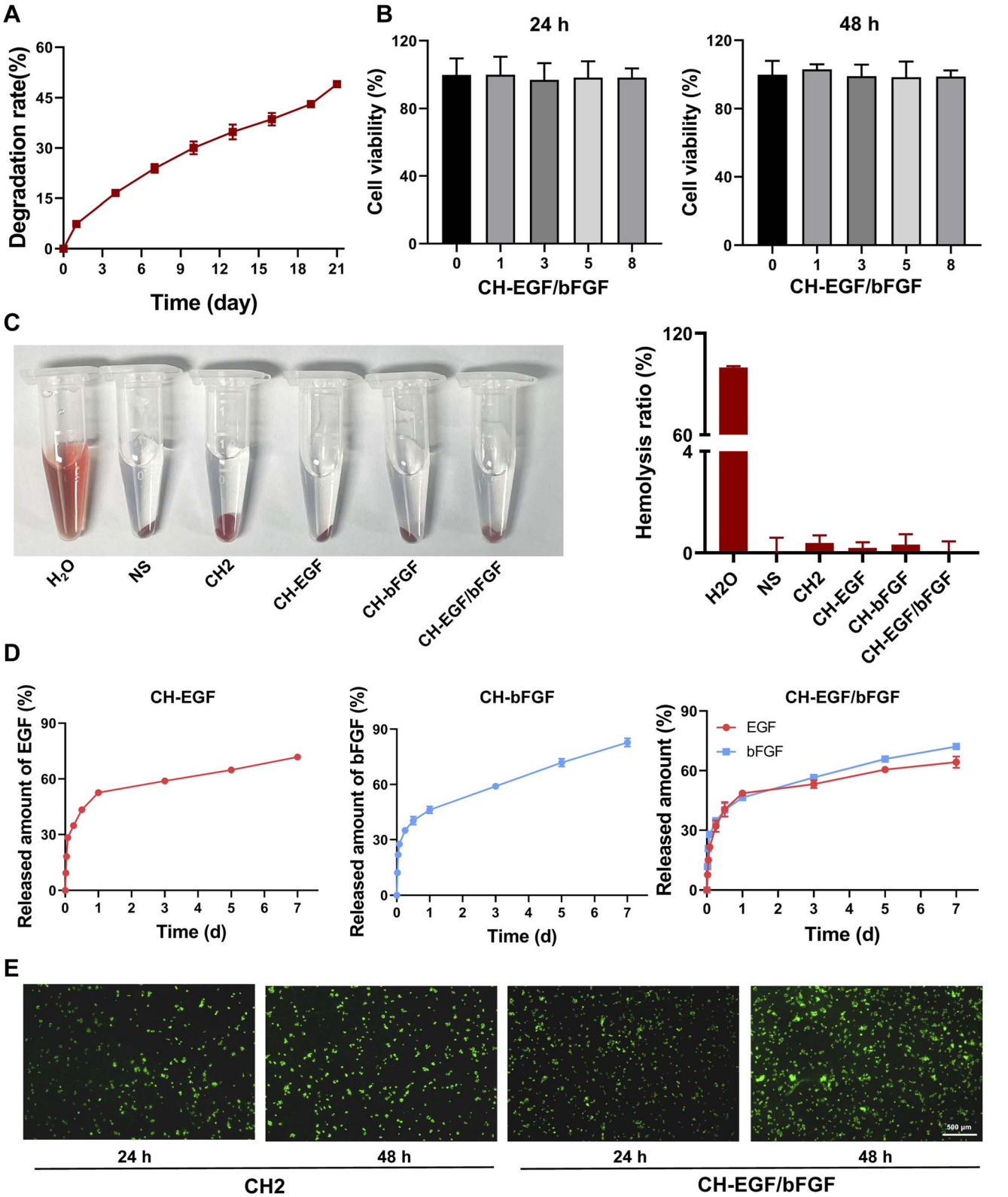

Fig. 2 Determination of the biological safety and wound repair capability of CH-EGF/bFGF *in vitro*. (A) Detection of the biodegradation rate of CH-EGF/bFGF in PBS solution, $n = 3$. (B) Assessment of the effects of CH-EGF/bFGF with different areas (0, 1 × 1 mm, 3 × 3 mm, 5 × 5 mm, 8 × 8 mm) on the viability of HaCaT cells using the CCK-8 method, $n = 3$. (C) Hemolysis test, $n = 3$. (D) Measurement of the release rates of bFGF and EGF from CH-EGF/bFGF using the ELISA method, $n = 3$. (E) Evaluation of the adhesion and growth of HaCaT cells on CH2 and CH-EGF/bFGF by FDA staining (scale bar, 500 μm), $n = 3$.

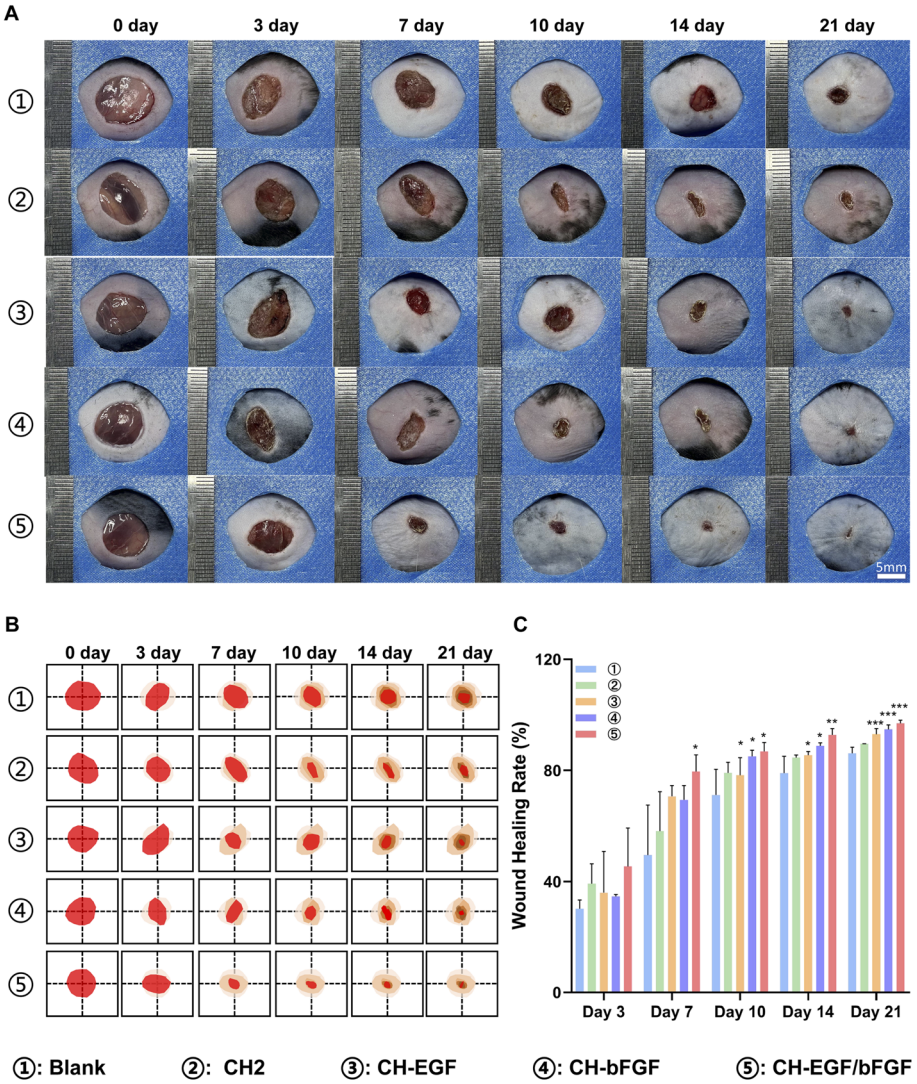

Fig. 3 CH-EGF/bFGF promoted wound healing in diabetic mice. (A) After treatment with CH-EGF/bFGF nanofiber membranes, the wound healing status of mice in each group was continuously monitored for 21 days, Scale bar = 5 mm, $n = 3$. (B and C) Statistical analysis of wound areas, $n = 3$. *$p < 0.05$, **$p < 0.01$, ***$p < 0.001$ *vs.* Blank group.

areas, there was an absence of tissue formation and growth. Seven days post-treatment, mice in the CH2 group displayed mild inflammatory responses in the skin. On the 21st day, varying degrees of recovery were observed in the epidermal structures of the wound tissues implanted with different dressings. When compared to the Blank group, the CH-EGF/bFGF group showed a relatively lower number of inflammatory cells but a higher number of fibroblasts. The epidermal layer was significantly thickened, and the epidermal tissue nearly completely covered the wound surface (Fig. 4A).

3.4. CH-EGF/bFGF enhanced collagen remodeling and angiogenesis

Collagen, as the primary component of the ECM in skin tissue, contributes to scar-free wound healing. Consequently, Masson staining was employed to measure the effect of CH-EGF/bFGF on collagen deposition, in order to further elucidate its promoting role in diabetic wound healing. The results showed that the Blank and CH2 groups had relatively low levels of collagen deposition during the healing process, while the CH-EGF/bFGF group exhibited a relatively high level of collagen deposition (Fig. 4B). This indicated that CH-EGF/bFGF promoted collagen formation, ECM remodeling, and skin tissue regeneration, thereby accelerating the healing of diabetic wounds.

Vascular endothelial growth factor (VEGF) is a specific mitogen for vascular endothelial cells, capable of stimulating the proliferation, migration, and lumen formation of vascular endothelial cells, thus playing a crucial role in the wound healing process.[18] By measuring the expression level of VEGF, it was found that, compared with the Blank group, the VEGF levels in different drug-treated groups were all significantly elevated. Among them, the CH-EGF/bFGF group showed the most pronounced increase in VEGF level, indicating that the

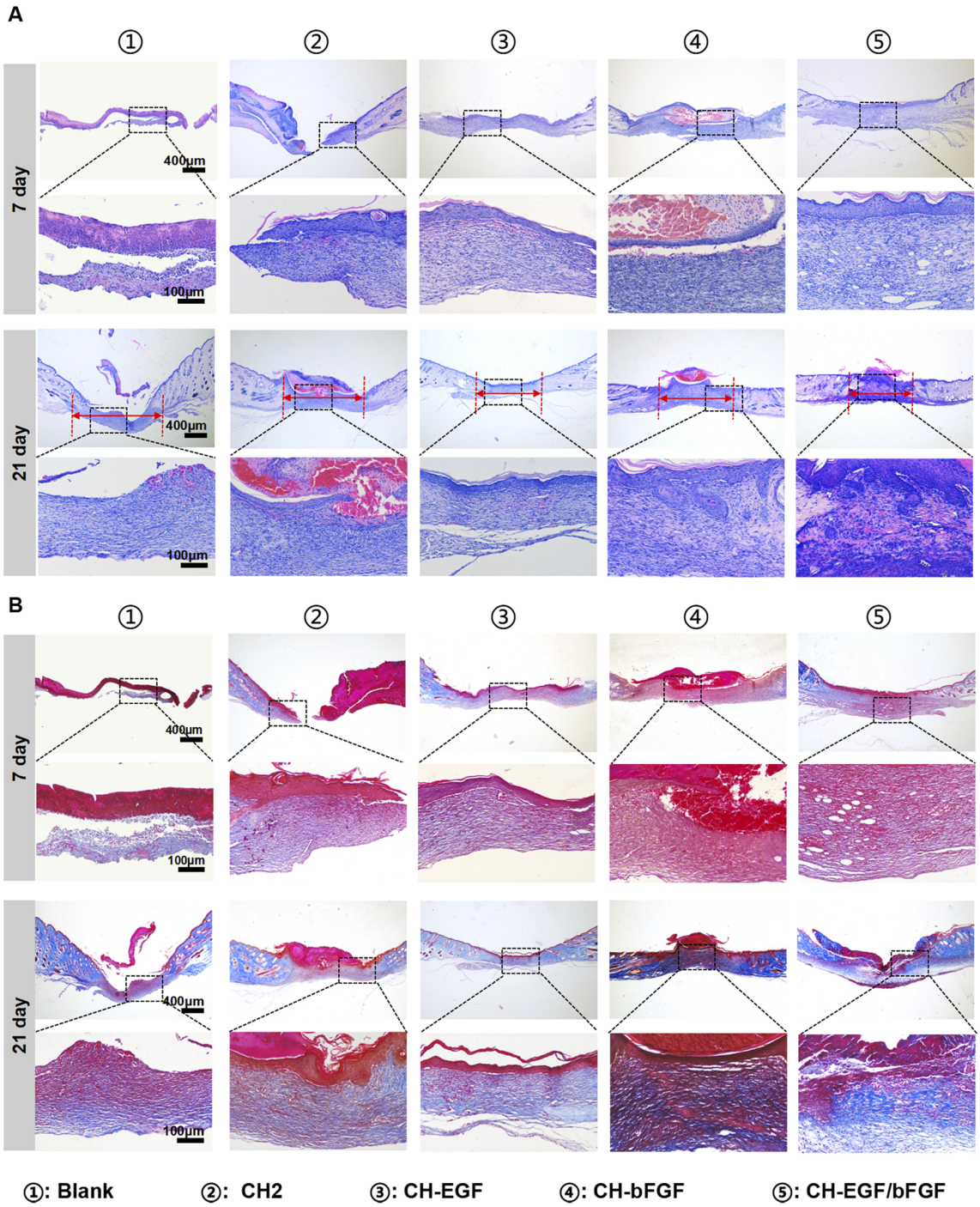

Fig. 4 CH-EGF/bFGF promoted wound healing and collagen deposition. (A) Representative H&E staining images showing wound healing status at the 7th and 21st days after treatment with different dressings, $n = 3$. (B) H&E staining illustrating collagen deposition in the wound areas after treatment with different dressings, $n = 3$.

intervention of CH-EGF/bFGF could promote wound healing by upregulating the expression of VEGF (Fig. 5A and B). In addition, to evaluate the effect of CH-EGF/bFGF on cell proliferation, IHC was employed to determine the expression level of Ki67 in the wound area. Ki67 is a nuclear antigen closely related to cell proliferation, and its expression level serves as an indicator of cellular proliferative activity. The intervention of CH-EGF/bFGF significantly increased the expression of Ki67 (Fig. 5A and C), promoting cell proliferation and accelerating wound healing.

Meanwhile, the expression of CD31 in the wound areas was measured. CD31, as an important marker of angiogenesis, can reflect the activity of vascular endothelial cells and the state of angiogenesis.[19] The results showed that the fluorescence intensity in the CH-EGF/bFGF group was significantly higher

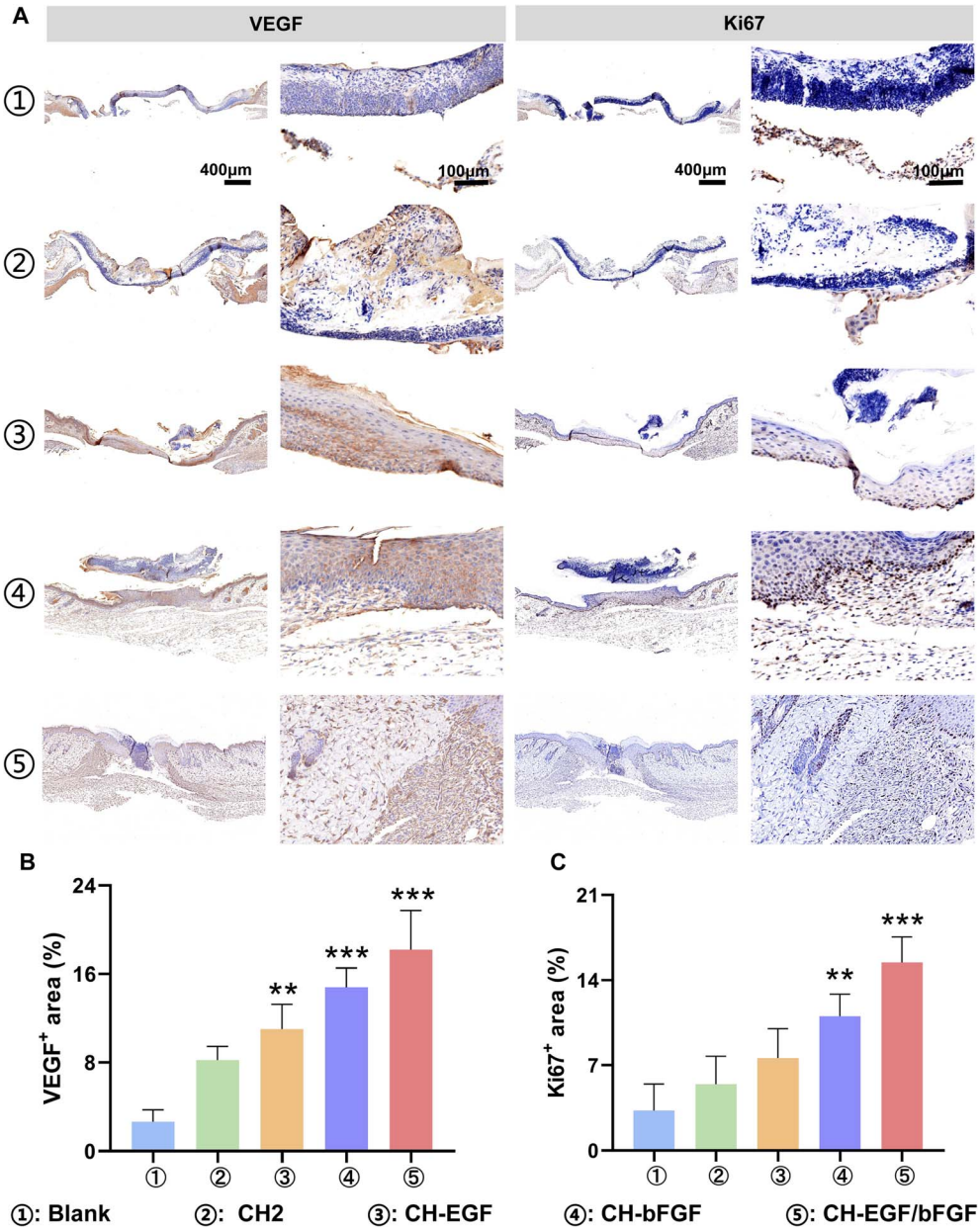

Fig. 5 CH-EGF/bFGF upregulated the expression of VEGF and Ki67. (A) Expression of VEGF and Ki67 in wound tissues treated with different drugs on the 7th day, $n = 3$. (B and C) Statistical analysis of the areas of VEGF and Ki67 expression, $n = 3$. *$p < 0.05$, **$p < 0.01$, ***$p < 0.001$ *vs.* Blank group.

than that in the Blank group, indicating that CH-EGF/bFGF can effectively promote angiogenesis and thus accelerate wound healing (Fig. 6A and B).

In addition, α-SMA is a marker of myofibroblasts, which play a crucial role in the wound healing process. Myofibroblasts possess contractile ability, enabling them to contract the wound, reduce the wound area, and promote wound closure. High expression of α-SMA implies enhanced activity of myofibroblasts, which is conducive to promoting ECM remodeling and wound healing. Through the measurement of α-SMA expression (Fig. 6A and C), a similar conclusion was reached: CH-EGF/bFGF can significantly increase the expression of α-SMA and promote wound healing.

Collagen I serves as the primary structural protein in the skin, imparting strength and stability to tissues. The dense fibrous network formed by its deposition serves as the structural basis of the ECM. In contrast, Collagen III exhibits a more delicate fibrous structure. During the early stages of healing, it accelerates tissue repair by promoting fibroblast migration, vascular endothelial cell proliferation, and neovascularization. Through the measurement of the expression of Collagen I and Collagen III, it was found that during the early phase of healing (on the 7th day), the intervention of CH-EGF/bFGF significantly

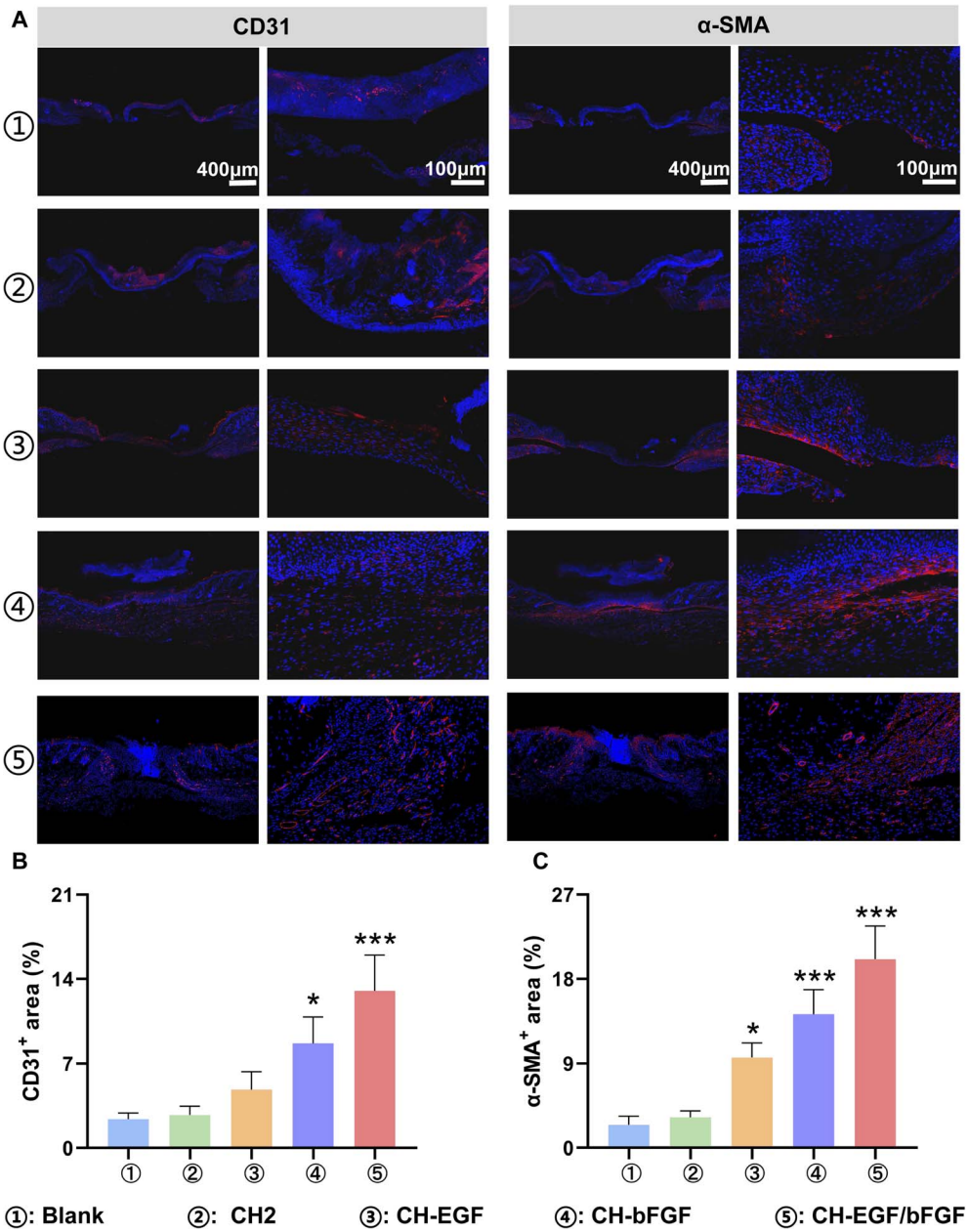

Fig. 6 Intervention with CH-EGF/bFGF upregulates the expression of CD31 and α-SMA. (A) Immunofluorescence assay was used to determine the expression of CD31 and α-SMA in the wound areas, $n = 3$. (B and C) Quantitative statistical analysis of the expression of CD31 and α-SMA was performed using Image J, $n = 3$. *$p < 0.05$, **$p < 0.01$, ***$p < 0.001$ *vs.* Blank group.

promoted the expression of both Collagen I and Collagen III, with Collagen III expression predominating (Fig. 7A–C). This high level of Collagen III expression was closely associated with active angiogenesis and rapid formation of granulation tissue. In the later stages of healing (on the 21st day), the expression of Collagen I became dominant in the CH-EGF/bFGF group, with the level of Collagen I taking the lead in the CH-EGF/bFGF group, while the expression of Collagen III decreased relative to Collagen I (Fig. 7D–F). This transition in collagen types signifies the completion of ECM remodeling. The increased proportion of mature collagen enhanced the mechanical strength of scar tissue.

3.5. CH-EGF/bFGF promotes keratinocyte proliferation and migration *in vitro*

To evaluate the effects of CH-EGF/bFGF on keratinocyte activity, HaCaT cells were treated with CH-EGF, CH-bFGF, or CH-EGF/bFGF membranes for 24 and 48 hours. CCK-8 assays demonstrated that all factor-loaded groups significantly enhanced cell viability compared with the Blank and CH2 groups, with CH-EGF/bFGF showing the most pronounced increase (Fig. 8A–C). Moreover, scratch wound assays revealed that CH-EGF/bFGF significantly accelerated HaCaT cell migration compared with CH-EGF, CH-bFGF, and control groups (Fig. 8D–E).

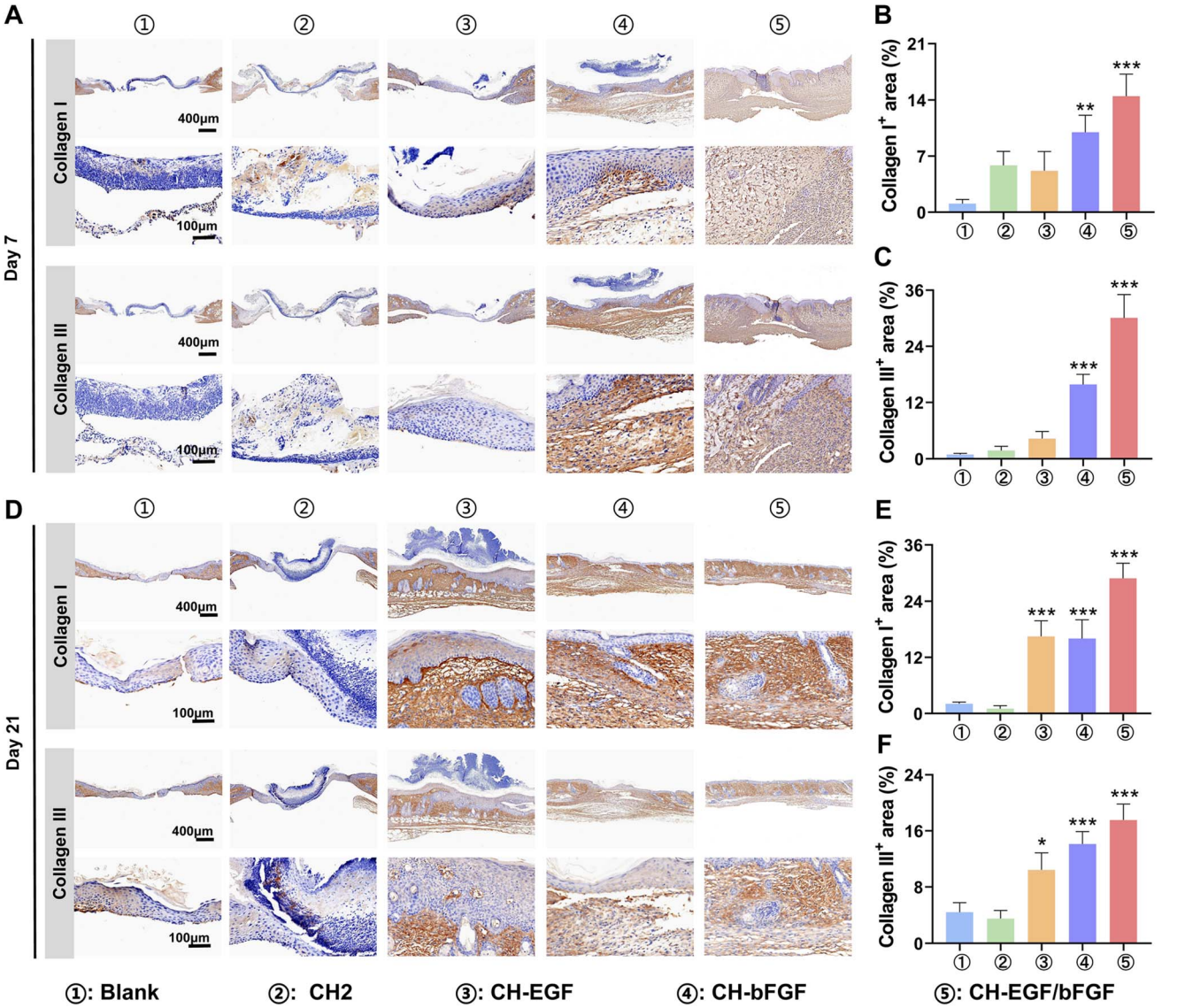

Fig. 7 CH-EGF/bFGF promoted the expression of Collagen I and Collagen III in wound areas. (A) IHC was used to determine the expression of Collagen I and Collagen III in wound areas on the 7th day, $n = 3$. (B and C) Statistical analysis of the expression of Collagen I and Collagen III in wound areas on the 7th day, $n = 3$. (D) IHC was used to determine the expression of Collagen I and Collagen III in wound areas on the 21st day, $n = 3$. (E and F) Quantitative measurement of the expression of Collagen I and Collagen III in wound areas on the 21st day using Image J, $n = 3$. *$p < 0.05$, **$p < 0.01$, ***$p < 0.001$ *vs.* Blank group.

Western blot analysis was performed to investigate the activation of ERK1/2 and p38 MAPK signaling pathways. As shown in Fig. 8F–G, the phosphorylation levels of ERK1/2 and p38 were markedly increased in the CH-EGF and CH-bFGF groups compared with the Control and CH2 groups. Notably, the CH-EGF/bFGF group exhibited a more pronounced increase in both p-ERK1/2/ERK1/2 and p-p38/p38 ratios compared with either the CH-EGF or CH-bFGF group alone.

4. Discussion

In this study, we elucidated that CH-EGF/bFGF exhibited favorable degradability and biosafety, promoted the adhesion and growth of HaCaT cells, and simultaneously accelerated wound healing in db/db mice, demonstrating promising potential for promoting diabetic wound healing. Wound healing encompasses dynamic processes such as the acute inflammatory phase, cellular proliferation phase, scar formation phase, and regeneration of the epidermis and other tissues.[20] However, regardless of the stage of wound healing, the process requires the regulation of multiple factors, including transforming growth factor-β (TGF-β), VEGF, bFGF, and EGF, among others. Nevertheless, diabetic wounds are characterized by various cellular dysfunctions, including impaired migration of keratinocytes and fibroblasts, defective T-cell immune function,[21] and upregulation of matrix metalloproteinases.[22] All these factors delay the healing process of diabetic wounds and may even lead to their deterioration. Additionally, the growth

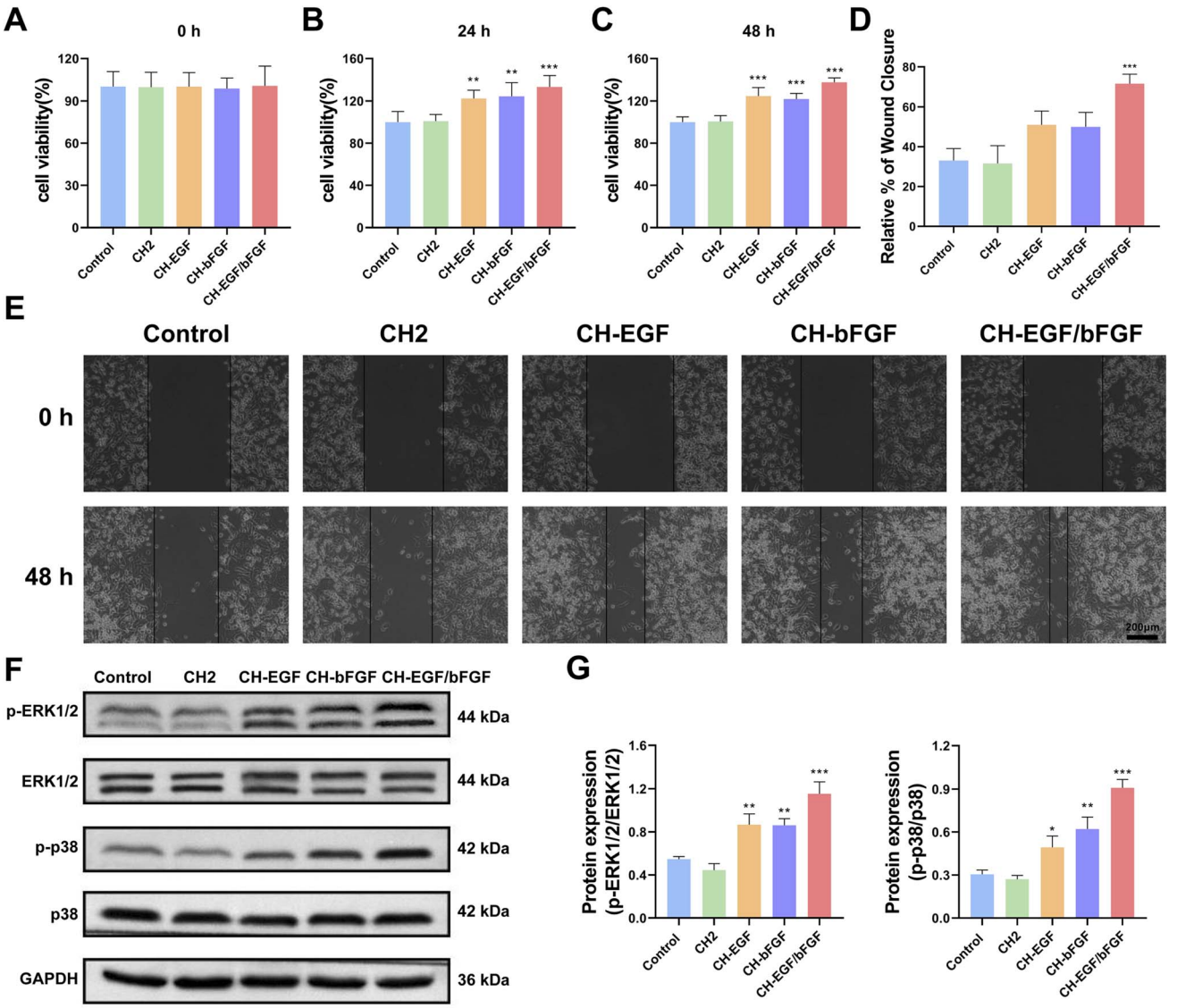

Fig. 8 *In vitro* validation of the effects of CH-EGF/bFGF on HaCaT cell proliferation and migration and its potential mechanisms. (A–C) Cell viability at 0 h, 24 h, and 48 h after corresponding treatments, $n = 3$. (D) Quantitative analysis of relative wound closure, $n = 3$. (E) Representative images of the wound healing assay, $n = 3$. (F) Western blot analysis of protein expression levels of p-ERK1/2, ERK1/2, p-p38, and p38, $n = 3$. (G) Quantitative analysis of relative protein expression levels. $n = 3$. $^{*}p < 0.05$, $^{**}p < 0.01$, $^{***}p < 0.001$ *vs.* Control group.

factors in diabetic patients are in a state of imbalance, further contributing to poor wound healing. Addressing the imbalance of growth factors may represent a therapeutic approach to promote diabetic wound healing. Among numerous growth factors, EGF has been reported to enhance re-epithelialization by promoting the migration and proliferation of keratinocytes. Meanwhile, bFGF has been shown to stimulate angiogenesis, thereby triggering wound healing. However, the short half-life and poor stability of EGF and bFGF limit their clinical applications.[23] Although various dosage forms such as ointments and intralesional injections are available on the market, these products still have issues in terms of drug distribution, bioavailability, and stability of EGF and bFGF.[24] Therefore, we prepared CH2 as a drug carrier for EGF and bFGF using electrospinning technology, achieving controlled release of these two critical growth factors over a period of 1–7 days. The preparation of this carrier enhanced the stability of both EGF and bFGF and prolonged the drug administration duration, providing a potential strategy for the treatment of diabetic non-healing wounds.

Electrospun nanofibers have been widely investigated for wound dressing applications due to their ECM-like architecture and favorable mass transfer properties.[25,26] In this study, electrospinning technology was employed to prepare CH1, CH2, and CH3 in order to screen the optimal collagen I/HA ratio and construct a dual-factor delivery system. Among the tested formulations, CH2 exhibited the most balanced physicochemical and mechanical properties. Compared with CH1 and CH3, CH2 showed moderate stiffness combined with superior elongation at break, indicating improved structural adaptability to

dynamic wound environments. In addition, the optimized fiber diameter and uniform network structure of CH2 may provide a microenvironment more suitable for cell adhesion, migration, and proliferation. Meanwhile, the excellent hydrophilicity of the CH2 membrane can be attributed to both its material composition and microstructural characteristics. The relatively high HA content provides abundant hydrophilic functional groups, while type I collagen contributes polar amino acid residues that can interact with water molecules. In addition, the electrospun fibrous network with uniform fiber diameter and interconnected pores further enhances water absorption and retention. This enhanced water absorption and retention capacity helps maintain a moist wound microenvironment, which is essential for keratinocyte migration and granulation tissue formation. These combined properties may explain why CH2 served as an optimal carrier for growth factor loading and wound repair support. Importantly, the release profile of CH-EGF/bFGF demonstrated sustained release behavior during the first 1–7 days, which may correspond well to the early inflammatory and proliferative phases of wound healing. During early-stage diabetic wound repair, rapid activation of keratinocytes, fibroblasts, and endothelial cells is required, which is highly dependent on growth factor signaling. The relatively faster initial release of EGF and bFGF may help rapidly activate cell proliferation and angiogenesis-related pathways. Subsequently, the slower release phase may support continued ECM remodeling, fibroblast activity, and vascular maturation during later healing stages. This stage-adaptive release pattern may partially explain the superior therapeutic efficacy observed in the CH-EGF/bFGF group.

Recent advances in wound dressing design indicate a paradigm shift from passive protective materials toward multifunctional bioactive platforms that integrate structural biomimicry, controlled drug delivery, and microenvironmental modulation.[27] Emerging studies suggest that nanostructured delivery systems can enhance drug stability and optimize release kinetics,[28] while mechanically adaptive dressings can better match tissue dynamics and accelerate wound closure.[27] In addition, multifunctional nanoplatforms with antibacterial or antibiofilm capabilities can further improve healing outcomes.[29,30] In this context, the CH-EGF/bFGF system developed in this study provides an ECM-mimicking nanofibrous architecture combined with sustained dual growth factor release, enabling the simultaneous regulation of cellular behavior, angiogenesis, and extracellular matrix remodeling. CH-EGF/bFGF effectively promoted the growth and migration of HaCaT cells and accelerated wound healing in db/db mice. Specifically, in the early inflammatory phase, the rapid release of EGF and bFGF helps activate keratinocytes and fibroblasts, and may also modulate local immune cell activity, which is critical for clearing pathogens and debris.[20] In the subsequent proliferative phase, EGF enhances keratinocyte proliferation and migration to promote re-epithelialization, while bFGF stimulates endothelial cells to form new capillaries and supports fibroblast-mediated ECM deposition. During the scar formation phase, the dual delivery of EGF and bFGF maintains fibroblast activity and collagen synthesis, optimizing tissue architecture. Finally, in the regeneration and remodeling phase, the combined effects of EGF and bFGF contribute to collagen maturation, an increased Collagen I/Collagen III ratio, and functional tissue restoration. By coordinating these processes across the four stages of wound healing, CH-EGF/bFGF accelerates wound closure while improving tissue quality and vascularization.

Mechanistically, EGF can significantly upregulate the expression of endogenous epidermal growth factor receptor, subsequently binding to the receptor and activating downstream signaling pathways such as p38-MAPK/ERK1/2.[31] In the present study, we further explored the potential molecular mechanisms underlying the enhanced therapeutic efficacy of the CH-EGF/bFGF group. As evidenced by increased phosphorylation levels of ERK1/2 and p38, both EGF and bFGF could activate ERK1/2 and p38 MAPK signaling pathways. Importantly, the CH-EGF/bFGF group showed significantly higher activation levels compared with either single-factor group. The ERK1/2 pathway plays a central role in regulating fibroblast proliferation, keratinocyte migration, and endothelial cell angiogenic activity, while the p38 MAPK pathway is closely associated with inflammatory regulation, collagen synthesis, and tissue remodeling. The enhanced activation of these pathways in the CH-EGF/bFGF group may explain the superior wound healing outcomes, including accelerated wound closure, increased vascular density, and enhanced collagen deposition observed in this study. Besides, we assessed the proliferation and viability of myofibroblasts by measuring the expression of α-SMA and Ki67. The results demonstrated that treatment with CH-EGF/bFGF upregulated the expression of both α-SMA and Ki67, suggesting that this system might effectively promote diabetic wound healing by activating myofibroblasts and enhancing their proliferative potential. Furthermore, previous studies have indicated that EGF and bFGF can promote neovascularization by inducing the production of VEGF in cells.[32] This conclusion was corroborated in our study, where we determined the expression of VEGF through IHC. The results showed that treatment with CH-EGF/bFGF significantly increased VEGF expression and promoted angiogenesis, as evidenced by the upregulation of CD31 expression. These findings suggested that CH-EGF/bFGF may effectively accelerate angiogenesis, improve local microcirculation, and thereby collectively contribute to diabetic wound healing through multiple processes, including cell proliferation, granulation tissue formation, and angiogenesis. Quantitative comparison further supported the enhanced therapeutic efficacy of dual growth factor delivery. By day 14, the wound healing rate in the CH-EGF/bFGF group reached 92.81 ± 2.31%, which was approximately 7.30% and 3.92% higher than those observed in the CH-EGF (85.51 ± 1.30%) and CH-bFGF (88.89 ± 1.07%) groups, respectively. These results suggest that the combined delivery of EGF and bFGF may provide greater biological stimulation of key wound healing processes compared with single-factor delivery. Although these findings demonstrate enhanced combined therapeutic efficacy, further studies using factorial experimental designs would be required to determine

whether true biological synergy exists between the two growth factors.

Notably, CH-EGF/bFGF can upregulate the expression of both Collagen I and Collagen III. This effect was likely attributable to the therapeutic role played by bFGF. Specifically, bFGF can effectively stimulate fibroblasts to synthesize ECM components, such as collagen and fibronectin.[33] Meanwhile, bFGF may also promote collagen deposition and accelerate ECM remodeling by upregulating the levels of matrix metalloproteinases.[34] During the early stages of wound healing, Collagen III predominates, while Collagen I takes the lead in the later stages. This dynamic change aligns with the physiological pattern of normal wound healing. Collagen III serves as a "temporary scaffold" that provides elastic support for early repair, whereas the continuous deposition of Collagen I confers long-term stability to the healing tissue.[35] Additionally, an increase in the Collagen I/Collagen III ratio is positively correlated with ECM maturity.[36] By optimizing the temporal sequence of collagen metabolism, CH-EGF/bFGF achieved a balance between scar quality and tissue function.[37]

In this study, although the potential capability of the CH-EGF/bFGF dressing in promoting diabetic wound healing has been verified, our research was primarily centered on evaluating its therapeutic effects, while the exploration of its underlying mechanisms remained limited. In the present study, we found that the activation of the p38-MAPK and ERK1/2 pathways was associated with the acceleration of diabetic wound healing mediated by CH-EGF/bFGF. As mentioned earlier, CH-EGF/bFGF may exert its therapeutic effects through multiple pathways. These mechanisms work synergistically to promote cell proliferation, migration, and collagen production, thereby accelerating the healing of diabetic wounds. Considering the current inadequacies in research on its mechanisms of action, it is necessary to conduct more in-depth and comprehensive experimental studies in the future to further elucidate the precise mechanisms by which CH-EGF/bFGF dressings promote diabetic wound healing, providing a more solid theoretical basis for their clinical application.

5. Conclusion

In summary, a CH2-EGF/bFGF dressing was prepared, and it was demonstrated that this dressing could effectively promote wound healing in type 2 diabetic mice, demonstrating potential as a dressing for diabetic wounds. By integrating dual growth factor delivery with an ECM-mimicking nanofibrous platform, this work establishes a scientifically innovative and translationally promising strategy for diabetic wound management.

Ethical statement

This study was approved by the Experimental Animal Ethics Committee of Wenzhou Medical University (wydw2024-0588).

Author contributions

Liang Wu: writing-original draft, methodology, investigation, formal analysis, funding acquisition. Wei Wang: writing-original draft, methodology, investigation, formal analysis. Linxinyi Chen: methodology, investigation, formal analysis. Duohui Li: investigation, data curation, visualization. Yijun Ke: investigation, data curation, visualization. Yanghui Xu: investigation, data curation. Bo Zhu: investigation, data curation. Fangqi Hu: writing-review & editing, supervision. Lishang Dai: writing-review & editing, supervision, project administration. Xiwu Shi: writing-review & editing, supervision.

Conflicts of interest

The authors declare that they have no known competing financial interests or personal relationships that could have appeared to influence the work reported in this paper.

Data availability

Data can be obtained from the corresponding author without any restrictions.

Supplementary information (SI): Fig. S1: SEM observation of the effect of spinning voltage on fiber formation at (A) 6 kV, (B) 8 kV, (C) 12 kV, and (D) 14 kV. Fig. S2: the release rates of bFGF and EGF from CH-EGF/bFGF over 21 days were measured using ELISA. $n = 3$. See DOI: https://doi.org/10.1039/d5ra09378c.

Acknowledgements

This study was supported by the Research Project of Anhui Provincial Health Science and Technology Project (AHWJ2023A30066).

References

1 A. Vargas, G. Garcia, K. Rivara, K. Woodburn, L. E. Clemens and S. I. Simon, *Int. J. Mol. Sci.*, 2023, **24**, 2143.
2 N. R. Tshiluka, D. T. Mbedzi, M. V. Bvumbi and S. S. Mnyakeni-Moleele, *ChemistryOpen*, 2025, **14**, e202400119.
3 N. N. Mahmoud, S. Hamad and S. Shraim, *ACS Omega*, 2024, **9**, 44860–44875.
4 S. Y. Zheng, X. X. Wan, P. A. Kambey, Y. Luo, X. M. Hu, Y. F. Liu, J. Q. Shan, Y. W. Chen and K. Xiong, *World J Diabetes*, 2023, **14**, 364–395.
5 J. Berlanga-Acosta, A. Garcia-Ojalvo, J. Fernandez-Montequin, V. Falcon-Cama, N. Acosta-Rivero, G. Guillen-Nieto, M. Pujol-Ferrer, M. Limonta-Fernandez, M. Ayala-Avila and E. Eriksson, *Int. J. Mol. Sci.*, 2024, **25**, 10883.
6 C. Sun, Y. Huang, L. Wang, J. Deng, R. Qing, X. Ge, X. Han, G. Zha, W. Pu, B. Wang and S. Hao, *Int. J. Biol. Macromol.*, 2024, **261**, 129725.
7 X. Zhang, R. Hao, J. Tong, H. Hu, J. Du, B. Gong, F. Tian, Y. Lu and J. Xue, *Biomaterials*, 2026, **327**, 123797.

8 F. Huang, T. Gao, Y. Feng, Y. Xie, C. Tai, Y. Huang, L. Ling and B. Wang, *ACS Appl. Mater. Interfaces*, 2024, **16**, 45989–46004.
9 L. Huang, H. Chen, J. Nie, Y. Zhao and J. Miao, *Eur. J. Pharmacol.*, 2025, **987**, 177201.
10 I. Garcia-Orue, E. Santos-Vizcaino, J. Uranga, K. de la Caba, P. Guerrero, M. Igartua and R. M. Hernandez, *J. Mater. Chem. B*, 2023, **11**, 6896–6910.
11 L. Miao, X. Lu, Y. Wei, J. Zhou, Y. Liu, Y. Zhang, C. Meng, M. Li, H. Zhang, W. Chen and H. Zhang, *Mater Today Bio*, 2025, **31**, 101578.
12 Y. Wang, Y. Zhang, Y. P. Yang, M. Y. Jin, S. Huang, Z. M. Zhuang, T. Zhang, L. L. Cao, X. Y. Lin, J. Chen, Y. Z. Du, J. Chen and W. Q. Tan, *Bioact Mater*, 2024, **35**, 330–345.
13 J. Siminska-Stanny, D. Podstawczyk, C. Delporte, L. Nie and A. Shavandi, *Adv Healthc Mater*, 2024, **13**, e2402045.
14 S. Parmal, P. Subbappa, V. Nikam, Y. Tarwate, K. Barhate, S. Wagh, A. D. Gholap, K. Dua, S. K. Singh, D. Parikh, M. Shaikh, T. K. Khan and A. Rajput, *Int. J. Biol. Macromol.*, 2025, **306**, 141625.
15 D. Singh, V. Rai and D. K. Agrawal, *Cardiol Cardiovasc Med*, 2023, **7**, 5–16.
16 M. Rodriguez-Aguilar, B. Segura-Pacheco, B. Campillo-Illanes, M. S. Cordova-Aguilar, H. Merchant-Larios, S. Alcala-Alcala and A. Meneses-Acosta, *Polymers*, 2025, **17**, 2325.
17 R. Hao, H. Hu, X. Ye, X. Chen, J. Du, S. Li, C. Song, F. Tian, N. Zhao, F. Xu, T. Zhang, F. Rao and J. Xue, *Bioact Mater*, 2025, **52**, 200–212.
18 C. Lee, M. J. Kim, A. Kumar, H. W. Lee, Y. Yang and Y. Kim, *Signal Transduct Target Ther*, 2025, **10**, 170.
19 X. Shi, Y. Zhou, B. Du, X. Yao and X. Du, *J Wound Care*, 2024, **33**, 866–874.
20 Z. H. Deng, Z. L. Yang, S. Yi and Z. Q. Liu, *Eur. Cells Mater.*, 2025, **53**, 82–97.
21 T. Wei, T. Pan, X. Peng, M. Zhang, R. Guo, Y. Guo, X. Mei, Y. Zhang, J. Qi, F. Dong, M. Han, F. Kong, L. Zou, D. Li, D. Zhi, W. Wu, D. Kong, S. Zhang and C. Zhang, *Nat. Nanotechnol.*, 2024, **19**, 1178–1189.
22 J. Chen, S. Qin, S. Liu, K. Zhong, Y. Jing, X. Wu, F. Peng, D. Li and C. Peng, *Front Immunol*, 2023, **14**, 1089001.
23 Y. Kim, S. Jeon, B. Kim, Y. J. Jeong, T. H. Kim, S. Jeong, I. Kim, J. Oh, Y. Jung, K. Lee, Y. B. Choy, S. W. Kim and J. J. Chung, *ACS Appl. Mater. Interfaces*, 2025, **17**, 445–466.
24 K. Shakhakarmi, J. E. Seo, S. Lamichhane, C. Thapa and S. Lee, *Arch Pharm Res*, 2023, **46**, 299–322.
25 E. J. Jang, R. Patel and M. Patel, *Pharmaceutics*, 2023, **15**, 1144.
26 S. Liu, G. Wu, W. Wang, H. Wang, Y. Gao and X. Yang, *Mar. Drugs*, 2023, **21**, 241.
27 P. Zhang, Z. Liu, H. Pei, A. Ahmed, Y. Wei and D. Huang, *Acta Biomater.*, 2025, **208**, 168–189.
28 W. Ding, T. Zhang, R. Fu, C. Yu, C. Zhang, K. Wang and P. Zhang, *Chem. Eng. J.*, 2025, **516**, 163905.
29 P. Zhang, X. Chen, F. Bu, C. Chen, L. Huang, Z. Xie, G. Li and X. Wang, *ACS Appl. Mater. Interfaces*, 2023, **15**, 9926–9939.
30 J. Wu, X. Huo, J. Liu, F. Bu and P. Zhang, *Colloids Surf., B*, 2025, **245**, 114330.
31 D. Y. Shu, A. E. K. Hutcheon, J. D. Zieske and X. Guo, *Sci. Rep.*, 2019, **9**, 8079.
32 P. Lorenc, A. Sikorska, S. Molenda, N. Guzniczak, H. Dams-Kozlowska and A. Florczak, *Biomed Pharmacother*, 2024, **180**, 117585.
33 D. H. Bian, Y. Wu and G. D. Song, *Mater. Today Commun.*, 2023, **35**, 105876.
34 Y. Tu, Y. Li, G. Qu, Y. Ning, B. Li, G. Li, M. Wu, S. Li and Y. Huang, *J Biomed Mater Res A*, 2025, **113**, e37834.
35 L. Gardeazabal and A. Izeta, *Exp Dermatol*, 2024, **33**, e15052.
36 L. Li, Y. Ma, G. He, S. Ma, Y. Wang and Y. Sun, *Biomed Pharmacother*, 2023, **161**, 114510.
37 L. H. Li, Y. Y. Zha, M. Y. Liu, X. D. Hong, Y. J. Ding, Y. Zhou, H. H. Fei-yang, A. F. Chen, X. D. Zhang, Z. L. Chen and J. Jin, *J Burn Care Res*, 2024, **45**, 1269–1273.